



**HAL**  
open science

## Distinguishing Different Stackings in Layered Materials via Luminescence Spectroscopy

Matteo Zanfognini, Alexandre Plaud, Ingrid Stenger, Frédéric Fossard,  
Lorenzo Sponza, Léonard Schué, Fulvio Paleari, Elisa Molinari, Daniele  
Varsano, Ludger Wirtz, et al.

► **To cite this version:**

Matteo Zanfognini, Alexandre Plaud, Ingrid Stenger, Frédéric Fossard, Lorenzo Sponza, et al.. Distinguishing Different Stackings in Layered Materials via Luminescence Spectroscopy. *Physical Review Letters*, 2023, 131 (20), pp.206902. 10.1103/physrevlett.131.206902 . hal-04292218

**HAL Id: hal-04292218**

**<https://hal.science/hal-04292218>**

Submitted on 17 Nov 2023

**HAL** is a multi-disciplinary open access archive for the deposit and dissemination of scientific research documents, whether they are published or not. The documents may come from teaching and research institutions in France or abroad, or from public or private research centers.

L'archive ouverte pluridisciplinaire **HAL**, est destinée au dépôt et à la diffusion de documents scientifiques de niveau recherche, publiés ou non, émanant des établissements d'enseignement et de recherche français ou étrangers, des laboratoires publics ou privés.

## Distinguishing Different Stackings in Layered Materials via Luminescence Spectroscopy

Matteo Zanfagnini,<sup>1,2</sup> Alexandre Plaud,<sup>3,4</sup> Ingrid Stenger<sup>4</sup>, Frédéric Fossard<sup>3</sup>, Lorenzo Sponza<sup>3</sup>, Léonard Schué,<sup>3,4</sup> Fulvio Paleari<sup>2,\*</sup>, Elisa Molinari<sup>1,2</sup>, Daniele Varsano<sup>2</sup>, Ludger Wirtz,<sup>5</sup> François Ducastelle,<sup>3</sup> Annick Loiseau,<sup>3,†</sup> and Julien Barjon<sup>4,‡</sup>

<sup>1</sup>*Dipartimento di Scienze Fisiche, Informatiche e Matematiche, Università di Modena e Reggio Emilia, I-41125 Modena, Italy*

<sup>2</sup>*Centro S3, CNR-Istituto Nanoscienze, I-41125 Modena, Italy*

<sup>3</sup>*Université Paris-Saclay, ONERA, CNRS, Laboratoire d'étude des microstructures, 92322 Châtillon, France*

<sup>4</sup>*Université Paris-Saclay, UVSQ, CNRS, GEMaC, 78000 Versailles, France*

<sup>5</sup>*Department of Physics and Materials Science, University of Luxembourg, 1511 Luxembourg, Luxembourg*

(Received 29 May 2023; accepted 12 October 2023)

Despite its simple crystal structure, layered boron nitride features a surprisingly complex variety of phonon-assisted luminescence peaks. We present a combined experimental and theoretical study on ultraviolet-light emission in hexagonal and rhombohedral bulk boron nitride crystals. Emission spectra of high-quality samples are measured via cathodoluminescence spectroscopy, displaying characteristic differences between the two polytypes. These differences are explained using a fully first-principles computational technique that takes into account radiative emission from “indirect,” finite-momentum excitons via coupling to finite-momentum phonons. We show that the differences in peak positions, number of peaks, and relative intensities can be qualitatively and quantitatively explained, once a full integration over all relevant momenta of excitons and phonons is performed.

DOI:

The microscopic control of Van der Waals stacking configurations is emerging as an important tool for the engineering of the optoelectronic properties of layered materials. In graphite, for example, rhombohedral stacking may result in nontrivial topological properties [1], while the asymmetry of the interlayer coupling resulting from the same stacking motif leads to the emergence of ferroelectricity in transition metal dichalcogenides [2,3], as well as increased effective mobilities due to the change in interlayer coupling strength [4]. The local changes in stacking order in twisted boron nitride (BN) layers again give rise to ferroelectric domains [5]. Understanding the impact of single-layer stacking configurations on the electronic properties of Van der Waals materials is thus of paramount importance. Consequently, exploring BN polytypes serves as an exemplary platform for such investigations. Layered BN crystals are identified as strategic materials for the integration of graphene and 2D semiconductors in optoelectronic devices based on Van der Waals heterostructures [6–8]. To this end, largely scalable crystal growth methods able to produce high-quality samples are desirable. The highest-quality BN single crystals are mostly grown from a catalytic melt either at high pressure and high temperature [9–11] or, more recently, at intermediate or atmospheric pressure and high temperature [12–16]. The resulting crystals are limited in size or polycrystalline, which restricts their possible applications to optoelectronics. Up-scalable fabrication techniques at low pressure, such as chemical vapor deposition or molecular beam

epitaxy, allow instead for the controlled synthesis of BN thin films on large surfaces. However, they have encountered a limited success up to now due to the polymorphism of boron nitride. The layered bulk crystal can come, in principle, in six different polytypes [17], with the two most stable ones adopting the hexagonal (hBN) and rhombohedral (rBN) Bravais lattices. In hBN, two adjacent BN single layers differ by a  $\pi$  rotation, resulting in the so-called AA' stacking sequence, where boron and nitrogen atoms sit on top of each other [Fig. 1(a)]. Conversely, the unit cell of rBN crystals is composed of three BN monolayers, which are rigidly shifted along the same direction by the B-N planar interatomic distance: this stacking motif (ABC sequence) is shown in Fig. 1(b). While this stacking

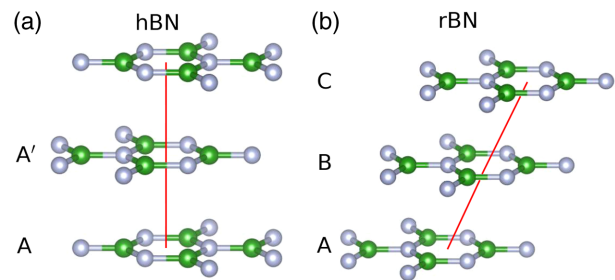


FIG. 1. Stacking sequences of  $sp_2$  BN considered in this work: in (a) boron nitride with AA' stacking is shown, while in (b) the three shifted layers forming rBN unit cell are presented. Nitrogen and boron atoms are shown in grey and green, respectively.

65 difference entails an extremely high energy cost associated  
 66 to the transformation from rBN to hBN [18], these two  
 67 polytypes are difficult to distinguish experimentally from a  
 68 crystallographic point of view. Even from a computational  
 69 point of view, the calculated stability difference of the  
 70 two polytypes is close to the limit of accuracy of modern  
 71 *ab initio* methods [17,19,20]. In addition, the interaction  
 72 with the substrate affects the abundance of stable rBN and  
 73 hBN phases in synthetic products [21–24]. For these  
 74 reasons, the stacking sequence is rarely characterized in  
 75 recent reports about BN multilayer growth, so that possible  
 76 differences in the respective optoelectronic properties of the  
 77 two polytypes might have been overlooked.

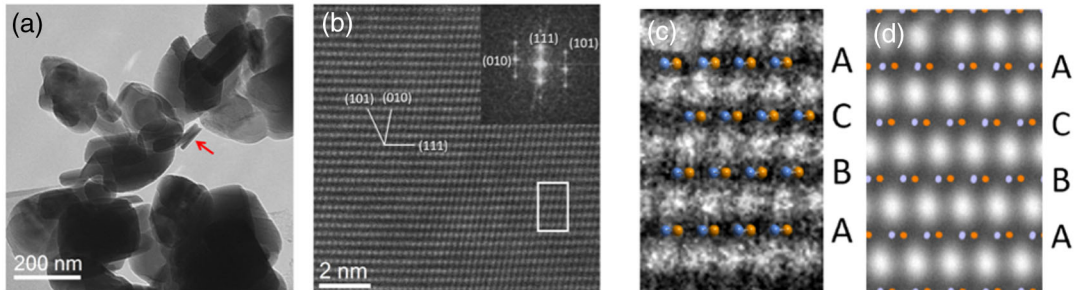
78 In this Letter, we present a spectroscopic investigation of  
 79 rBN using cathodoluminescence (CL) spectroscopy. By  
 80 comparing CL spectra obtained for rBN with analogous  
 81 results for hBN [25,26], we demonstrate that the stacking  
 82 sequence affects the emission fine structure of rBN and  
 83 hBN crystals, making CL an ideal experimental probe to  
 84 discriminate between the two polytypes. Our experimental  
 85 observations are explained by *ab initio* calculations of  
 86 luminescence spectra for the two polytypes, explicitly  
 87 including exciton-phonon interactions.

88 The reference sample investigated here is the rBN  
 89 powder fabricated by T. Sato [21], which is known as  
 90 the international standard for the crystallographic diffrac-  
 91 tion database [27]. To our knowledge, this is the highest-  
 92 quality rBN single crystal available today. Figure 2(a)  
 93 presents a transmission electron microscopy (TEM) image  
 94 of the powder. It consists of cylindrical rBN crystallites  
 95 with a typical 200 nm diameter and a 50 nm thickness. The  
 96 ABC stacking sequence can be observed in the high-  
 97 resolution image of the transverse section reported in  
 98 Fig. 2(b). The distance between B and N in this projection  
 99 is 0.072 nm, which cannot be resolved due to our 0.12 nm  
 100 TEM limit resolution. Nevertheless, the positions of B and  
 101 N atomic columns can be identified in Fig. 2(c) thanks to  
 102 simulations performed in the conditions of the image  
 103 acquisition in Fig. 2(d) (see Supplemental Material [28]

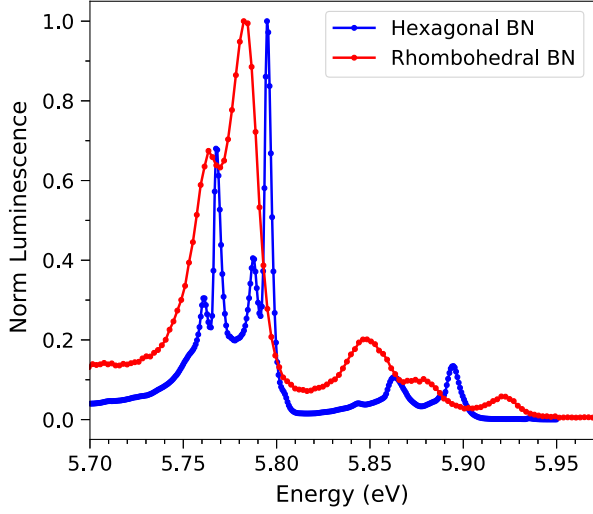
104 for details). The identification of the rBN structure is  
 105 further confirmed by comparing its Raman spectrum  
 106 with the one of hBN as presented in the Supplemental  
 107 Material [28] section on Raman spectroscopy. In the  
 108 following, the properties of the reference rBN sample  
 109 (ABC stacking) will be compared with a reference hBN  
 110 crystal grown by high pressure and high temperature [11].

111 We now turn to the discussion of the exciton-dominated  
 112 luminescence spectra as studied by CL using the setup  
 113 detailed in Supplemental Material [28]. A comparison  
 114 between the experimental CL spectra of hBN and rBN  
 115 at  $T = 5$  K is shown in Fig. 3. The visible features are due  
 116 to phonon-assisted excitonic recombinations as will be  
 117 discussed below. The two spectra display several key  
 118 differences, including a redshift of the rBN features with  
 119 respect to the corresponding hBN ones (which amounts to  
 120 15 meV for the highest peak), and, most importantly, the  
 121 presence of two relevant structures at 5.847 and 5.919 eV  
 122 only in rBN. The high accuracy of the experimental rBN  
 123 spectrum is crucial to clearly resolve the fine structure of  
 124 the intrinsic phonon-assisted peaks [17,42], enabling us to  
 125 explain these points in conjunction with the theoretical  
 126 modeling in the following. Experimentally, these reported  
 127 differences are fully significant, as we obtained almost  
 128 identical spectra from a rBN sample grown by chemical  
 129 vapor deposition on 6H-SiC. A detailed comparison  
 130 between the two samples is included in Supplemental  
 131 Material [28], along with a discussion of the defect peaks  
 132 appearing in the CL signal measured at frequencies lower  
 133 than those shown in Fig. 3.

134 *Ab initio* calculations [43] indicate that rBN is an indirect  
 135 band-gap insulator. The exciton dispersion resulting from  
 136 the solution of the Bethe-Salpeter equation at finite  
 137 momentum is indirect as well, its minimum being located  
 138 near the point  $\Omega = [\frac{1}{6}, \frac{1}{6}, 0]$  in the middle of the  $\Gamma K$   
 139 symmetry direction in the hexagonal Brillouin zone  
 140 (hBZ). According to our calculation, the energy difference  
 141 between the lowest-lying exciton (due to indirect electronic  
 142 transition) and the optically accessible (i.e., direct and



F2:1 FIG. 2. (a) Bright field TEM image of the reference rBN powder. (b) High resolution TEM image in the  $[10\bar{1}]$  zone axis of the  
 F2:2 crystallite indicated by the red arrow in (a). The traces of (101), (001), and (111) rBN planes reported with white lines are identified with  
 F2:3 the Fourier transform plotted in inset. (c) Magnified image of the white rectangle in (b) where the atomic positions of B and N (colored  
 F2:4 spheres) are deduced from the simulation (d), which has been performed with the illumination conditions used experimentally.  
 F2:5 Crystallographic notations refer here to the rhombohedral phase (see Supplemental Material [28] for details).



F3:1 FIG. 3. Comparison of experimental hBN (blue) and rBN (red)  
 F3:2 CL spectra at  $T = 5$  K.

143 dipole-allowed)  $\Gamma$  excitons is 230 meV (see Supplemental  
 144 Material [28] for the exciton dispersion curve computed  
 145 along this direction). This means that the excitonic radiative  
 146 recombination in rBN requires the assistance of phonons  
 147 with a wave vector around the  $\Omega$  point, similarly to what  
 148 happens in hBN.

149 The theoretical luminescence spectra have been computed  
 150 using the expression [44,45]

$$I(E) \propto \sum_{\lambda} \sum_{\mathbf{Q}} \sum_{\nu} N[E_{\lambda}(\mathbf{Q})] \Gamma_{\lambda}^{\nu, \mathbf{Q}}(E), \quad (1)$$

152 where  $\lambda$  is an index running over exciton bands,  $\mathbf{Q}$  is the  
 153 exciton momentum, and  $\nu$  denotes the phonon branches.  
 154  $N[E_{\lambda}(\mathbf{Q})] = e^{-[(E_{\lambda}(\mathbf{Q}) - \mu)/k_B T_{\text{exc}}]}$  is a Boltzmann distribution  
 155 representing the exciton population from which light  
 156 emission occurs,  $\mu$  being the energy of the lowest-energy  
 157 exciton in the system and  $T_{\text{exc}}$  the effective excitonic  
 158 temperature. We fixed  $T_{\text{exc}}$  to 20 K, which is its exper-  
 159 imental value obtained for low sample temperatures (below  
 160 10 K, as in Fig. 3). (We have checked that our results are  
 161 stable with respect to small changes of this parameter).

162 The probability  $\Gamma_{\lambda}^{\nu, \mathbf{Q}}(E)$  describes photon emission by a  
 163 finite-momentum exciton  $|\lambda, \mathbf{Q}\rangle$ , assisted by a phonon  
 164  $(\nu, \mathbf{Q})$ . This quantity has been computed using second-  
 165 order time-dependent perturbation theory, similarly to  
 166 Refs. [46,47], only considering phonon emission processes  
 167 [48] (which dominate at small temperature):

$$\Gamma_{\lambda}^{\nu, \mathbf{Q}}(E) = |T_{\lambda}^{\nu, \mathbf{Q}}|^2 \frac{(1 + n_{\nu, \mathbf{Q}}) \delta[E - E_{\lambda}(\mathbf{Q}) + \hbar\omega_{\nu, \mathbf{Q}}]}{E_{\lambda}(\mathbf{Q}) - \hbar\omega_{\nu, \mathbf{Q}}}, \quad (2)$$

168 with

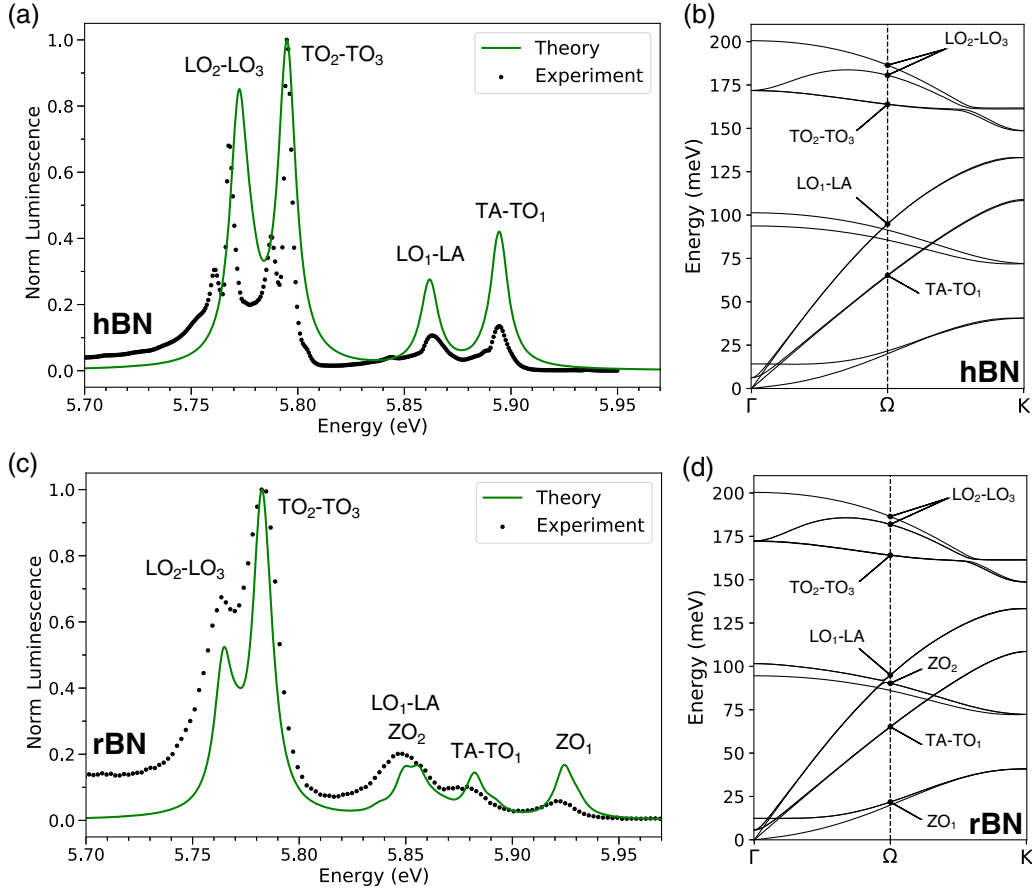
$$T_{\lambda}^{\nu, \mathbf{Q}} = \sum_{\lambda_2} \frac{D_{\lambda_2} G_{\lambda_2, \lambda}^{\nu}(\mathbf{Q}, -\mathbf{Q})}{E_{\lambda_2}(\Gamma) + \hbar\omega_{\nu, \mathbf{Q}} - E_{\lambda}(\mathbf{Q})}. \quad (3)$$

In Eqs. (2) and (3), the index  $\lambda_2$  runs over the excitonic  
 170 states at the  $\Gamma$  point with energy  $E_{\lambda_2}(\Gamma)$ . The quantity  $D_{\lambda_2}$   
 172 is the excitonic optical dipole strength averaged over in-plane  
 173 polarization directions.  $n_{\nu, \mathbf{Q}}$  corresponds to the Bose-  
 174 Einstein phonon occupation factor, while  $E$  is the energy  
 175 of the emitted photon; the Dirac delta guarantees energy  
 176 conservation and has been numerically approximated with  
 177 a Lorentzian function with FWHM equal to 5 meV in order  
 178 to match the experimental peaks. Finally, the exciton-  
 179 phonon coupling matrix element  $G_{\lambda_2, \lambda}^{\nu}(\mathbf{Q}, -\mathbf{Q})$  describes  
 180 the scattering amplitude for an exciton  $|\lambda, \mathbf{Q}\rangle$  to states  
 181  $|\lambda_2, \Gamma\rangle$  while assisted by phonon mode  $\nu$  [45]:  
 182

$$G_{\lambda_2, \lambda}^{\nu}(\mathbf{Q}, -\mathbf{Q}) = \sum_{vc'k} A_{\lambda_2}^{*\Gamma}(v\mathbf{k}, c\mathbf{k}) A_{\lambda}^{\mathbf{Q}}(v\mathbf{k}, c'\mathbf{k} + \mathbf{Q}) g_{cc'}^{\nu}(\mathbf{k} + \mathbf{Q}; -\mathbf{Q}) - \sum_{vv'ck} A_{\lambda_2}^{*\Gamma}(v\mathbf{k}, c\mathbf{k}) A_{\lambda}^{\mathbf{Q}}(v'\mathbf{k} - \mathbf{Q}, c\mathbf{k}) g_{v'v}^{\nu}(\mathbf{k}; -\mathbf{Q}), \quad (4)$$

where  $A_{\lambda}^{\mathbf{Q}}(v\mathbf{k}_h, c\mathbf{k}_c)$  is the envelope function for exciton  
 183  $|\lambda, \mathbf{Q}\rangle$ , with  $v, v'$  ( $c, c'$ ) running over the valence (con-  
 185 duction) states and  $\mathbf{k}$  being the electronic wave vector in the  
 186 hBZ. The electron-phonon coupling matrix element  
 187  $g_{n,n'}^{\nu}(\mathbf{k}, \mathbf{Q})$  represents the scattering between single-particle  
 188 states  $|n', \mathbf{k}\rangle$  and  $|n, \mathbf{k} + \mathbf{Q}\rangle$  [49]. Importantly, within our  
 189 numerical methodology,  $G_{\lambda_2, \lambda}^{\nu}(\mathbf{Q}, -\mathbf{Q})$  is computed using  
 190 the same single-particle Kohn-Sham states both for elec-  
 191 tron-phonon and excitonic quantities, thus overcoming  
 192 phase mismatch problems as described in Ref. [47]. The  
 193  $\mathbf{Q}$  integration appearing in Eq. (1) has been performed in  
 194 local neighborhoods of the symmetry-equivalent  $\Omega$  points  
 195 corresponding to the excitonic dispersion minima in the  
 196 hBZ. The computational details [50] needed to reproduce  
 197 the theoretical results are provided in the Supplemental  
 198 Material [28].  
 199

In Fig. 4, we present the comparison between exper-  
 200 imental CL spectra (black dots) and theoretical Bethe-  
 201 Salpeter equation results (continuous green lines) for hBN  
 202 [Fig. 4(a)] and rBN (Fig. 4(c)). Figures 4(b) and 4(d) show  
 203 the calculated in-plane phonon dispersion along the  $\Gamma\text{K}$   
 204 direction for hBN and rBN, respectively. We find very good  
 205 agreement between experimental and theoretical data. The  
 206 relative energy shift between the two spectra is reproduced  
 207 theoretically. As the phonon energies in the two systems  
 208 differ only for a few meV, the 15 meV shift closely matches  
 209 the underlying difference between the lowest-lying, finite-  
 210 momentum exciton levels (which is around 12 meV). In  
 211 turn, this difference can be traced back to the combined  
 212 effects of rBN having both a smaller quasiparticle band gap  
 213 (by 166 meV) and exciton binding energy (by 150 meV)  
 214



F4:1 FIG. 4. Experimental (black dots) and theoretical (green lines) luminescence spectra for hBN (a) and  
 F4:2 rBN (c). In both (a) and (c), theoretical spectra are blueshifted by 1.04 eV to match the position of the highest intensity peak in the experimental spectrum (in order to  
 F4:3 compensate for the systematic theoretical undercorrection of the *GW* quasiparticle band gap in BN). Phonon dispersions in hBN (b) and  
 F4:4 rBN (d) along the  $\Gamma$ -K direction: phonon branches contributing to the luminescence spectra are highlighted at the  $\Omega$  point, in the middle  
 F4:5 of the  $\Gamma$ -K direction. See the main text for the phonon mode labeling. Almost-degenerate phonon branches are paired with a hyphen.

215 with respect to hBN around the  $\Omega$  points in momentum  
 216 space. In both hBN and rBN, the spectra are dominated by  
 217 the two peaks in the low-energy part of the spectrum. These  
 218 are phonon-assisted satellites due to longitudinal optical  
 219 phonons—denoted as  $LO_2$ - $LO_3$  modes in the phonon  
 220 dispersion—and transverse optical ones (the almost-  
 221 degenerate pair [56]  $TO_2$ - $TO_3$ ). For hBN, these assign-  
 222 ments are in good agreement with the results obtained  
 223 in Refs. [46,57], using a finite-difference approach.  
 224 Furthermore, the experimental intensity ratio between these  
 225 peaks is well-reproduced by *ab initio* calculations, with the  
 226 LO peak being less intense than the TO one. The additional  
 227 overtones appearing in the measurements in this energy  
 228 region are due to higher-order scattering processes [58] and  
 229 are thus not captured by our theoretical approach, which is  
 230 restricted to first-order exciton-phonon interaction. The  
 231 phonon branches involved in the emission process are  
 232 explicitly labeled in Figs. 4(b) and 4(d) for the  $\Omega$  point  
 233 only [59]. Luminescence spectra of hBN and rBN are  
 234 qualitatively different at higher energies, as confirmed by  
 235 *ab initio* results. In the case of hBN, we observe only two

236 main peaks: the first (at about 5.86 eV) corresponds to a  
 237 replica of the  $LO_1$ -LA phonons, while the higher intensity  
 238 structure at 5.89 eV is mainly due to TO phonons, with a  
 239 small contribution from the almost-degenerate transverse  
 240 acoustic mode ( $TA$ - $TO_1$ ). *Ab initio* results reproduce with  
 241 great accuracy both the splitting between these peaks and  
 242 their intensity ratio (the  $LO_1$ -LA peak being less pro-  
 243 nounced than the  $TO_1$ - $TA$  one), while they tend to  
 244 overestimate their relative strengths, with respect to the  
 245 dominant, low-energy satellites. [The agreement may be  
 246 further improved with a more complete  $\mathbf{Q}$ -point integration  
 247 in Eq. (1).] We also note that, in agreement with the group  
 248 theory analysis discussed in Ref. [57], no contributions  
 249 from the out-of-plane phonon modes appear in the lumi-  
 250 nescence spectra. This selection rule, which is strictly  
 251 respected by Eq. (4), can be slightly broken in a real  
 252 experiment, leading to the appearance of a very small signal  
 253 corresponding to this mode (usually 100 times smaller than  
 254 the other peaks [60]).

255 In the case of rBN, the high-energy portion of the CL  
 256 spectrum shows three large peaks, respectively at about

257 5.847, 5.878, and 5.919 eV, instead of the two peaks  
 258 appearing in hBN. They are also recovered in the *ab initio*  
 259 results. The first structure is a combination of phonon-  
 260 assisted replicas due to the almost-degenerate LA-LO<sub>1</sub>  
 261 branches, albeit with a relevant contribution from optical  
 262 out-of-plane modes (denoted as ZO<sub>2</sub>; see Supplemental  
 263 Material [28] for a mode-resolved spectrum). Conversely,  
 264 the peak at 5.878 eV is associated to the TA-TO<sub>1</sub> phonons  
 265 in analogy with the hBN case. We emphasize that *ab initio*  
 266 results correctly reproduce the intensity ratio among these  
 267 peaks. Finally, the highest-energy structure at 5.919 eV  
 268 turns out to be due to the out-of-plane optical mode ZO<sub>1</sub>.  
 269 This is forbidden for the centrosymmetric hBN lumines-  
 270 cence while it is allowed in the rBN case because of the  
 271 lowered symmetry of the crystal lattice.

272 In conclusion, we have demonstrated that cathodolumi-  
 273 nescence is a viable tool to characterize fundamentally  
 274 similar BN polytypes, which are hardly distinguishable  
 275 otherwise. We have explained both experimentally and  
 276 theoretically how the radiative emission spectrum is  
 277 affected by the interaction between electronic excitations  
 278 and lattice vibrations in rhombohedral and hexagonal boron  
 279 nitride, two prototypical polytypes of low-dimensional  
 280 layered materials with indirect band gap. Using a first-  
 281 principles methodology that accounts for exciton-phonon  
 282 interactions beyond the state of the art, we are able to  
 283 provide a comprehensive and accurate description of the  
 284 finite-momentum exciton states and phonon modes  
 285 involved, thus showing the discriminating role of out-of-  
 286 plane lattice vibrations assisting excitonic radiative recom-  
 287 bination for rBN but not for hBN. We believe that our  
 288 analysis and methodology could be useful for the growth  
 289 and characterization of indirect-gap layered materials,  
 290 which find widespread application as basic building blocks  
 291 in novel 2D optoelectronic devices.

292 The authors would like to thank C. Vilar for the technical  
 293 support on electron microscopy and K. Watanabe and  
 294 T. Taniguchi for kindly providing a part of the rBN  
 295 reference powder of T. Sato, M. Chubarov, and  
 296 A. Henry for providing rBN whiskers on 6H-SiC. We  
 297 thank C. Attacalite and P. Lechiffart for useful discus-  
 298 sions about exciton-phonon coupling calculations. This  
 299 project has received funding from the European Union  
 300 Horizon 2020 research and innovation programme under  
 301 Grant Agreements No. 785219 and No. 881603 (Graphene  
 302 Flagship core 2 and core 3), the French National Agency  
 303 for Research (ANR) under Grant Agreement No. ANR-14-  
 304 CE08-0018 (GoBN: Graphene on Boron Nitride  
 305 Technology), MaX—MAterials design at the eXascale—  
 306 a European Centre of Excellence funded by the European  
 307 Union’s program HORIZON-EUROHPC-JU-2021-COE-  
 308 01 (Grant No. 101093374). D. V. and M. Z. also acknowl-  
 309 edge financial support from ICSC—Centro Nazionale di  
 310 Ricerca in High Performance Computing, Big Data and

Quantum Computing, funded by European Union—  
 NextGenerationEU—PNRR and the Italian national  
 program PRIN2017 Grant No. 2017BZPKSZ. L. W.  
 acknowledges funding by Fond National de Recherche  
 (FNR), Luxembourg via project INTER/19/ANR/  
 13376969/ACCEPT. We acknowledge EuroHPC Joint  
 Undertaking for awarding us access to MeluXina at  
 LuxProvide, Luxembourg and CINECA for computational  
 resources, awarded via the ISCRAs grants.  
 A. P. and M. Z. contributed equally to this work.

- \*Corresponding author: fulvio.paleari@nano.cnr.it  
 †Corresponding author: annick.loiseau@onera.fr  
 ‡Corresponding author: julien.barjon@uvsq.fr
- [1] S. Slizovskiy, E. McCann, M. Koshino, and V. I. Fal’ko, *Commun. Phys.* **2**, 164 (2019).
  - [2] X. Wang, K. Yasuda, Y. Zhang, S. Liu, K. Watanabe, T. Taniguchi, J. Hone, L. Fu, and P. Jarillo-Herrero, *Nat. Nanotechnol.* **17**, 367 (2022).
  - [3] J. Liang, D. Yang, J. Wu, J. I. Dadap, K. Watanabe, T. Taniguchi, and Z. Ye, *Phys. Rev. X* **12**, 041005 (2022).
  - [4] X. Li, X. Shi, D. Marian, D. Soriano, T. Cusati, G. Iannaccone, G. Fiori, Q. Guo, W. Zhao, and Y. Wu, *Sci. Adv.* **9**, eade5706 (2023).
  - [5] C. R. Woods, P. Ares, H. Nevison-Andrews, M. J. Holwill, R. Fabregas, F. Guinea, A. K. Geim, K. S. Novoselov, N. R. Walet, and L. Fumagalli, *Nat. Commun.* **12**, 347 (2021).
  - [6] K. S. Novoselov, A. Mishchenko, A. Carvalho, and A. H. C. Neto, *Science* **353**, aac9439 (2016).
  - [7] A. Geim and I. Grigorieva, *Nature (London)* **499**, 419 (2013).
  - [8] G. Wang, C. Robert, M. M. Glazov, F. Cadiz, E. Courtade, T. Amand, D. Lagarde, T. Taniguchi, K. Watanabe, B. Urbaszek, and X. Marie, *Phys. Rev. Lett.* **119**, 047401 (2017).
  - [9] V. L. Y. Solozhenko, I. A. Petrusha, and A. A. Svirid, *High Press. Res.* **15**, 95 (1996).
  - [10] K. Watanabe, T. Taniguchi, and H. Kanda, *Nat. Mater.* **3**, 404 (2004).
  - [11] T. Taniguchi and K. Watanabe, *J. Cryst. Growth* **303**, 525 (2007).
  - [12] Y. Kubota, K. Watanabe, O. Tsuda, and T. Taniguchi, *Science* **317**, 932 (2007).
  - [13] S. Liu, R. He, L. Xue, J. Li, B. Liu, and J. H. Edgar, *Chem. Mater.* **30**, 6222 (2018).
  - [14] M. Onodera, T. Taniguchi, K. Watanabe, M. Isayama, S. Masubuchi, R. Moriya, and T. Machida, *Nano Lett.* **20**, 735 (2020).
  - [15] J. Sonntag, J. Li, A. Plaud, A. Loiseau, J. Barjon, J. H. Edgar, and C. Stampfer, *2D Mater.* **7**, 031009 (2020).
  - [16] C. Maestre, Y. Li, V. Garnier, P. Steyer, S. Roux, A. Plaud, A. Loiseau, J. Barjon, L. Ren, C. Robert, B. Han, X. Marie, C. Journet, and B. Toury, *2D Mater.* **9**, 035008 (2022).
  - [17] B. Gil, W. Desrat, A. Rousseau, C. Elias, P. Valvin, M. Moret, J. Li, E. Janzen, J. H. Edgar, and G. Cassabois, *Crystals* **12**, 782 (2022).
  - [18] W. J. Yu, W. M. Lau, S. P. Chan, Z. F. Liu, and Q. Q. Zheng, *Phys. Rev. B* **67**, 014108 (2003).

- 371 [19] K. Luo, X. Yuan, Z. Zhao, D. Yu, B. Xu, Z. Liu, Y. Tian, G. 424  
372 Gao, and J. He, *J. Appl. Phys.* **121**, 165102 (2017). 425  
373 [20] H. Pedersen, B. Alling, H. Högborg, and A. Ektarawong, *J.* 426  
374 *Vac. Sci. Technol. A* **37**, 040603 (2019). 427  
375 [21] T. Sato, *Proc. Jpn. Acad. Ser. B* **61**, 459 (1985). 428  
376 [22] P. Sutter, J. Lahiri, P. Zahl, B. Wang, and E. Sutter, *Nano* 429  
377 *Lett.* **13**, 276 (2013). 430  
378 [23] A. Henry, M. Chubarov, Z. Czígány, M. Garbrecht, and H. 431  
379 Högborg, *Jpn. J. Appl. Phys.* **55**, 05FD06 (2016). 432  
380 [24] L. Souqui, J. Palisaitis, N. Ghafoor, H. Pedersen, and H. 433  
381 Högborg, *J. Vac. Sci. Technol. A* **39**, 013405 (2021). 434  
382 [25] G. Cassaboïs, P. Valvin, and B. Gil, *Nat. Photonics* **10**, 262 435  
383 (2016). 436  
384 [26] L. Schué, L. Sponza, A. Plaud, H. Bensalah, K. Watanabe, 437  
385 T. Taniguchi, F. Ducastelle, A. Loiseau, and J. Barjon, *Phys.* 438  
386 *Rev. Lett.* **122**, 067401 (2019). 439  
387 [27] Sample (f) in Ref. [21] is known under No 00-045-1171 for 440  
388 the Joint Committee on Powder Diffraction Standards 441  
389 (JCPDS) <http://www.icdd.com>. 442  
390 [28] See Supplemental Material at [http://link.aps.org/](http://link.aps.org/supplemental/10.1103/PhysRevLett.000.000000) 443  
391 [supplemental/10.1103/PhysRevLett.000.000000](http://link.aps.org/supplemental/10.1103/PhysRevLett.000.000000) for com- 444  
392 parisons between the CL spectrum of a different rBN 445  
393 sample, Raman spectra of hBN and rBN, TEM details, 446  
394 defect discussion, and computational details on the *ab initio* 447  
395 density functional theory, density functional perturbation 448  
396 theory, and exciton-phonon calculations including addi- 449  
397 tional data, which includes Refs. [29–41]. 450  
398 [29] L. Schue, Ph.D. thesis, Université Paris-Saclay, 2017. 451  
399 [30] M. Chubarov, H. Pedersen, H. Högborg, A. Henry, and Z. 452  
400 Czígány, *J. Vac. Sci. Technol. A* **33**, 061520 (2015). 453  
401 [31] J. Liu, Y. K. Vohra, J. T. Tarvin, and S. S. Vagarali, *Phys.* 454  
402 *Rev. B* **51**, 8591 (1995). 455  
403 [32] M. van Setten, M. Giantomassi, E. Bousquet, M. Verstraete, 456  
404 D. Hamann, X. Gonze, and G.-M. Rignanese, *Comput.* 457  
405 *Phys. Commun.* **226**, 39 (2018). 458  
406 [33] S. Baroni, S. de Gironcoli, A. Dal Corso, and P. Giannozzi, 459  
407 *Rev. Mod. Phys.* **73**, 515 (2001). 460  
408 [34] G. Onida, L. Reining, and A. Rubio, *Rev. Mod. Phys.* **74**, 461  
409 601 (2002). 462  
410 [35] K. Watanabe, T. Taniguchi, T. Kuroda, and H. Kanda, *Appl.* 463  
411 *Phys. Lett.* **89**, 141902 (2006). 464  
412 [36] P. Jaffrennou, J. Barjon, J.-S. Lauret, B. Attal-Trétout, F. 465  
413 Ducastelle, and A. Loiseau, *J. Appl. Phys.* **102**, 116102 (2007). 466  
414 [37] A. Pierret, H. Nong, F. Fossard, B. Attal-Trétout, Y. Xue, D. 467  
415 Golberg, J. Barjon, and A. Loiseau, *J. Appl. Phys.* **118**, 468  
416 234307 (2015). 469  
417 [38] L. Bourgeois, Y. Bando, and T. Sato, *J. Phys. D* **33**, 1902 (2000). 470  
418 [39] H. Prevost, A. Andrieux-Ledier, N. Dorval, F. Fossard, J. S. 471  
419 Mérot, L. Schué, A. Plaud, E. Héripéré, J. Barjon, and A. 472  
420 Loiseau, *2D Mater.* **7**, 045018 (2020). 473  
421 [40] F. Libbi, Pedro Miguel M. C. de Melo, Z. Zanolli, M. J. 474  
422 Verstraete, and N. Marzari, *Phys. Rev. Lett.* **128**, 167401 475  
423 (2022). 476
- [41] P. Stadelmann, *Ultramicroscopy* **21**, 131 (1987). 424  
[42] M. Moret, A. Rousseau, P. Valvin, S. Sharma, L. Souqui, H. 425  
Pedersen, H. Högborg, G. Cassaboïs, J. Li, J. H. Edgar, and 426  
B. Gil, *Appl. Phys. Lett.* **119**, 262102 (2021). 427  
[43] L. Sponza, H. Amara, C. Attacalite, S. Latil, T. Galvani, F. 428  
Paleari, L. Wirtz, and F. Ducastelle, *Phys. Rev. B* **98**, 429  
125206 (2018). 430  
[44] F. Paleari, Ph. D. thesis, University of Luxembourg, 2019. 431  
[45] H.-Y. Chen, D. Sangalli, and M. Bernardi, *Phys. Rev. Lett.* 432  
**125**, 107401 (2020). 433  
[46] E. Cannuccia, B. Monserrat, and C. Attacalite, *Phys. Rev.* 434  
*B* **99**, 081109(R) (2019). 435  
[47] P. Lechiffart, F. Paleari, D. Sangalli, and C. Attacalite, 436  
*Phys. Rev. Mater.* **7**, 024006 (2023). 437  
[48] G. P. G. Grosso, *Solid State Physics* (Academic Press, 438  
New York, 2000). 439  
[49] F. Giustino, *Rev. Mod. Phys.* **89**, 015003 (2017). 440  
[50] The theoretical spectra have been obtained using Quantum 441  
Espresso [51,52] and PERTURBO [53] packages to evaluate 442  
ground state electronic properties, vibrational excitations, 443  
and electron-phonon matrix elements while exciton energies 444  
and wave functions have been obtained using YAMBO 445  
[54,55] code. 446  
[51] P. Giannozzi *et al.*, *J. Phys. Condens. Matter* **21**, 395502 447  
(2009). 448  
[52] P. Giannozzi *et al.*, *J. Phys. Condens. Matter* **29**, 465901 449  
(2017). 450  
[53] J.-J. Zhou, J. Park, I.-T. Lu, I. Maliyov, X. Tong, 451  
and M. Bernardi, *Comput. Phys. Commun.* **264**, 107970 452  
(2021). 453  
[54] A. Marini, C. Hogan, M. Grüning, and D. Varsano, *Comput.* 454  
*Phys. Commun.* **180**, 1392 (2009). 455  
[55] D. Sangalli *et al.*, *J. Phys. Condens. Matter* **31**, 325902 456  
(2019). 457  
[56] A. Molina-Sánchez and L. Wirtz, *Phys. Rev. B* **84**, 155413 458  
(2011). 459  
[57] F. Paleari, H. P. C. Miranda, A. Molina-Sánchez, and L. 460  
Wirtz, *Phys. Rev. Lett.* **122**, 187401 (2019). 461  
[58] T. Q. P. Vuong, G. Cassaboïs, P. Valvin, V. Jacques, R. 462  
Cuscó, L. Artús, and B. Gil, *Phys. Rev. B* **95**, 045207 463  
(2017). 464  
[59] In our labeling of the phonon modes, we chose to disen- 465  
tangle explicitly the almost-degenerate Davydov pairs of 466  
modes. This is the reason why, for example, we consider the 467  
lowest-energy phonon mode to be a pair of acoustic (ZA) 468  
and optical ( $ZO_1$ ) out-of-plane modes, with only the latter 469  
being responsible for the signal in Fig. 4(c). In the 470  
experimental literature, this pair is usually labeled jointly 471  
as “ZA,” and the same goes for the other pairs. 472  
[60] T. Q. P. Vuong, G. Cassaboïs, P. Valvin, V. Jacques, A. V. D. 473  
Lee, A. Zobelli, K. Watanabe, T. Taniguchi, and B. Gil, *2D* 474  
*Mater.* **4**, 011004 (2016). 475  
476